High-Speed Low-Complexity Optical PAM Links With a High-Slope-Efficiency Optical Modulator: Analysis and Demonstration

Paikun Zhu, *Member, IEEE*, Yuya Yamaguchi, *Member, IEEE*, Yuki Yoshida, *Member, IEEE*, Pham Tien Dat, *Member, IEEE*, Masayuki Motoya, Shingo Takano, Ryo Shimizu, Kouichi Akahane, and Ken-ichi Kitayama, *Life Fellow, IEEE*

Abstract*—Achieving high data rate with simple system configuration and low power consumption is of great interest in short-reach intensity-modulation direct-detection (IM-DD) fiber links for future datacenter networks, business local area networks and so forth. For external modulation-based IM-DD, recently remarkable modulator performance has been achieved in terms of 3 dB bandwidth, exploiting different materials/platforms. However, due to the relatively-high RF-to-RF (or end-to-end) signal loss, optical amplifiers (OA) and/or RF amplifiers (RFA) were typically needed for IM-DD links, which increases the complexity and power dissipation. In this work, we present a more comprehensive figure of merit (FoM) for modulator (and link) design, namely "slope efficiency (SLE)", which takes into account not only the bandwidth but also the half-wave voltage and the RF/optical waveguide losses, and can provide a guiding principle of the modulator design toward lower RF-to-RF signal loss. With a high-SLE modulator, both OA and RFA can be omitted even when supporting broadband signals with CMOS-level driving voltages. We theoretically investigate the impact of modulators with different technology and SLE on the IM-DD pulse amplitude modulation (PAM) link. Next, we report a series of PAM transmission experiments with a high-SLE Lithium Niobate intensity modulator prototype, which enables sub-1V_{pp} driving, up-to-432 Gb/s PAM transmission over up-to-600 m single-mode fiber in C-band with OA&RFA-free reception and low digital signal processing (DSP) complexity. For instance, for 384 Gb/s PAM8 over 300 m, the transmitter was DSP-free while a symbol-spaced decision-feedback equalizer (DFE) with 61 feedforward taps and 1 feedback tap was sufficient for the receiver considering 16.7% hard-decision (HD)-FEC. Furthermore, we experimentally show that the high-SLE modulator supports ultra-wide fiber transmission bands (O-, S-, C- and L-band).

***Index Terms*—Direct detection (DD), optical modulator, pulse amplitude modulation (PAM), slope efficiency.**

Manuscript received 7 December 2023; revised 6 February 2024; accepted 12 February 2024. Date of publication 19 February 2024; date of current version 16 May 2024. This work was supported by JSPS KAKENHI under Grant 23K13340. *(Corresponding author: Paikun Zhu.)*

Paikun Zhu, Yuya Yamaguchi, Yuki Yoshida, Pham Tien Dat, and Kouichi Akahane are with the Optical Access Technology Laboratory, Network Research Institute, National Institute of Information and Communications Technology, Koganei 184-8795, Japan (e-mail: pkzhu3@nict.go.jp; yamaguchi@nict.go.jp; yuki@nict.go.jp; ptdat@nict.go.jp; akahane@nict.go.jp).

Masayuki Motoya, Shingo Takano, and Ryo Shimizu are with Sumitomo Osaka Cement Company, Ltd., Chiba 274-8601, Japan (e-mail: mmotoya@soc.co.jp; stakano@soc.co.jp; rshimizu@soc.co.jp).

Ken-ichi Kitayama is with Hamamatsu Photonics Central Research Laboratory, Hamamatsu 434-0041, Japan, and also with the National Institute of Information and Communications Technology, Koganei 184-8795, Japan (e-mail: kitayama@ieee.org).

Color versions of one or more figures in this article are available at https://doi.org/10.1109/JLT.2024.3366898.

Digital Object Identifier 10.1109/JLT.2024.3366898

I. Introduction

RESEARCH and development of high-speed short-reach fiber-optic communication systems based on intensity-modulation direct-detection (IM-DD) and related transceiver components have caught great interest in recent years, with potential applications of not only datacenter (DC) interconnects [1], [2], [3], [4], [5] but also future business local area networks [6] and mobile site cabling [7]. Compared with long-haul transmission, although the required data rate per lane of short-reach systems can also be high (e.g., beyond 300 Gb/s), the system should be designed to be considerably simpler with lower latency and power consumption. For examples, operating with CMOS-class driving voltages (1-V_{pp} (peak-to-peak voltage) or less [8]) is a laudable goal for an energy-efficient transmitter (Tx); the omitting of optical amplifier (OA) and radio-frequency (RF) amplifier (RFA) at the receiver (Rx) would be attractive to realize a lean system; pulse amplitude modulation (PAM) might be preferred over discrete multitone (DMT) to save a high-resolution wideband digital-to-analog converter (DAC) and to reduce Tx-side power consumption. For the digital signal processing (DSP), the equalizer should be implementation-friendly in addition to the bounded complexity, e.g., the number of feedback filter taps in the decision-feedback equalizer (DFE) for high-throughput DSP circuit may be restricted to 2 or less [9]. Moreover, some power-hungry forward error correction (FEC) schemes for long-haul transmissions, in particular with long codewords and/or iterative decoders, should be carefully discussed before being assumed for short-reach links.

An electro-optical modulation device is one of the key components for short-reach optical links. For systems using external modulation, e.g., via a Mach-Zehnder modulator (MZM), recently remarkable progress has been made on increasing their 3dB bandwidth for high-data-rate transmission [10], [11], [12], [13], [14], [15], [16], [17], [18]. These have been achieved by exploiting several materials/platforms, such as Lithium Niobate (LN), silicon photonics (SiPh), plasmonics, and hybrid ones. However, in most transmission demonstrations, OA and/or RFA were involved together with relatively heavy DSP, in order to

TABLE I
RECENT HIGH-SPEED (BEYOND-300 GB/S) IM/DD PAM TRANSMISSION DEMONSTRATIONS

Ref.	Line rate	E/O modulation device	Modulation format	SMF reach (km)	Num. of optical amplifiers	Num. of RF amplifiers	Need high-resolution DAC?	Digital filter & equalizer	NMpSec	FEC type, overhead
[10]	630-Gb/s	TFLN MZM	PS-PAM16 (RRC, α=0.01)	10 (w. DCF)	3	0	Y	2201-tap FFE@2-SpS,	8.8×10^{14}	SD, 26%
[11]	560-Gb/s	TFLN MZM	Faster-than-Nyquist PAM4	0.12	2	0	N	MF, ~1000-tap FFE@2-SpS, VNE, M-BCJR	1.8×10^{15}	HD, 20%
[12]	432-Gb/s	Plasmonic MZM	PAM8 (RC-shaped)	2.5 or 10 (w. DCF)	2	1	Y	PNE{301,41,41}, 7-tap DFE, BJCR	N/A	SD, 18.6%
[13]	370-Gb/s	Commercial LN MZM	PS-PAM16 (RC-shaped)	1	0	1	Y	PNE@2-SpS	6.9×10^{13}	SD, 21%
[14]	384-Gb/s	TFLN MZM	PS-PAM16 (RRC shaped, α=0.01)	0.5	1	2	Y	Tx: RRC, Rx: RRC, VNE{27,11,5}@2-SpS	1.6×10^{14}	SD, 27.5%
[15]	400-Gb/s	EML	PAM6 (RC-shaped)	0.1	0	2	Y	Tx: RC filter@4-SpS, Rx: DFE{99,99}	3.7×10^{13}	HD, 6.25%
[16]	369-Gb/s	Silicon MZM	PS-PAM8 (RC-shaped)	2 (O-band)	1	1	Y	Tx: RC & pre-emphasis filters; Rx: VNE	3.4×10^{13}	SD, 27.5%
[17]	430-Gb/s	TFLN MZM	PAM6 (RC-shaped)	0.12	1	0*	Y	Tx: RC & pre-emphasis filters; Rx: PNE	6.9×10^{13}	HD, 6.7%
This work	342-Gb/s	High-SLE LN MZM	PAM8	0.6	0	0*	N	LPF, DFE{91,1}	1.28×10^{13}	KP4-Hamming [42], 12.9%
	384-Gb/s		PAM8	0.3			N	LPF, DFE{61,1}	1.05×10^{13}	HD, 16.7%
	420-Gb/s		PAM8 (RRC shaped, α=0.02)	0.3			Y	Tx: RRC filter@2-SpS; Rx: RRC filter@2-SpS, 121-tap FFE	8.67×10^{13}	SD, 20%
	320-Gb/s		PAM6	2 (O-band)			N	LPF, DFE{61,1}	1.05×10^{13}	KP4-Hamming, 12.9%

* Operating at CMOS-compatible or sub-1V_{pp} driving voltages.
TFLN: thin-film LN. EML: electro-absorption modulated laser. SpS: sample-per-symbol. MF: matched filter. FFE: feedforward equalizer. DFE: decision-feedback equalizer. "DFE{*x,y*}" means DFE with *x* feedforward taps and *y* feedback taps. (R)RC: (root) raised-cosine. VNE/PNE: Volterra/polynomial nonlinear equalizer. "VNE/PNE{*x,y,z*}" means VNE/PNE with *x* linear taps, *y* 2nd-order nonlinear taps and *z* 3rd-order nonlinear taps. (M-) BJCR: (M-state) Bahl-Cocke-Jelinek-Raviv algorithm. LPF: (digital) low-pass filter. α: roll-off factor of the RC/RRC filter. SD: soft-decision. HD: hard-decision.

compensate for the RF-to-RF signal losses during the E/O and O/E conversion. This increased system complexity and energy consumption. It would be important to investigate in detail and to reduce such RF-to-RF signal loss in order to simplify the system.

In this work, we present a more comprehensive figure of merit (FoM), "slope efficiency (SLE)", which can be used to examine the modulator's performance at the system level and reveals the RF-to-RF signal loss. SLE was originally a FoM for directly-modulated semiconductor lasers, which is the incremental slope of laser power vs. laser current [19], [20]. In the radio-over-fiber (RoF) context, (generalized) SLE for optical modulators was derived and used to quantify the RF-to-RF signal gain/loss of an analog (passband) RoF link [20], [21], [22], [23]. Here, we leverage SLE to discuss modulator-based baseband high-speed IM-DD transmission links. SLE takes into account not only the bandwidth but also half-wave voltage V_π and RF/optical waveguide losses of modulators. Theoretical analysis and results show that the system/link performance can be competitive with a high-SLE modulator even if its 3dB bandwidth seems not advantageous. Following this design FoM, we fabricated and packaged an LN intensity modulator prototype. It has an insertion loss of $<$4 dB, $\approx$30 GHz 3 dB bandwidth but moderate roll-off to 100 GHz, and half-wave voltage of 1.9 V. It enables an average $>$6-dBm Tx output (with modulation) with only a 13 dBm laser, and further empowers sub-1V_{pp} driving, up-to-432-Gb/s N-ary pulse amplitude modulation (PAM-N) transmission over up-to-600 m (up to $\sim$10 ps/nm dispersion) single-mode fiber with OA&RFA-less reception and low DSP complexity. Specifically, the Tx is DSP-free (i.e., without any digital shaping or pre-emphasis filter) up to 384-Gb/s while the Rx-side equalizer to achieve the 16.7% HD-FEC limit for the 384-Gb/s signal is just a symbol-spaced DFE with 61 feedforward taps and 1 feedback tap. Table I provides a (non-exhaustive) summary of external modulation-based high-speed short-reach PAM demonstrations in recent years. Fig. 1(a) summarizes the DSP complexity (characterized by the number of real-valued multiplications per second (NMpSec) [24]) and bitrate-distance product (BDP) of these works. The calculation method for NMpSec of different DSP algorithms is listed in Fig. 1(b). With the high-SLE MZM, our demonstrated PAM link has about 70% reduction in NMpSec compared to prior art, meanwhile without requiring OA or RFA. Extended from our previous conference paper [25], this work additionally presents extensive experimental results together with in-depth discussions to support the work.

The rest of the paper is organized as follows. In Section II, we introduce the theoretical modeling of modulator's SLE and the IM-DD link, along with system error performance. Device design is also described. In Section III, experimental setup and results of up-to-432-Gb/s PAM transmissions are reported with discussions. Finally, Section IV concludes the work.

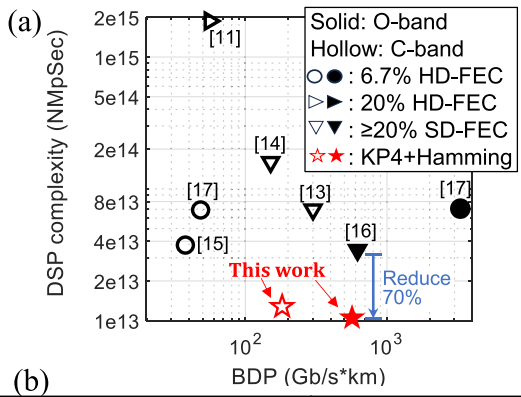

(b)

DSP algorithm	NMpSec
Linear filter (RC, RRC, FFE, …)	N_L*F_S
2nd-/3rd-order Volterra FFE	[N_L+N_{2nd}(N_{2nd}+1)+ N_{3rd}(N_{3rd}+1)(N_{3rd}+2)/2]*F_S
2nd-order polynomial FFE	(N_L+2*N_{2nd})*F_S
DFE	(N_L+N_{FB})*F_S
M-BJCR (for N-PAM)	L*M*N*F_S

Fig. 1. (a) NMpSec and (net) bitrate-distance product (BDP) of DCF-free short-reach IM-DD transmission demonstrations in C-band and O-band. When the DSP details of a previous work is not disclosed sufficiently, we made assumptions to show a conservative NMpSec. (b) DSP algorithms and their NMpSec. F_S: sampling rate of the DSP. N_L/N_{2nd}/N_{3rd}: number of linear/2nd-order/3rd-order taps. N_{FB}: number of feedback taps. L: memory length.

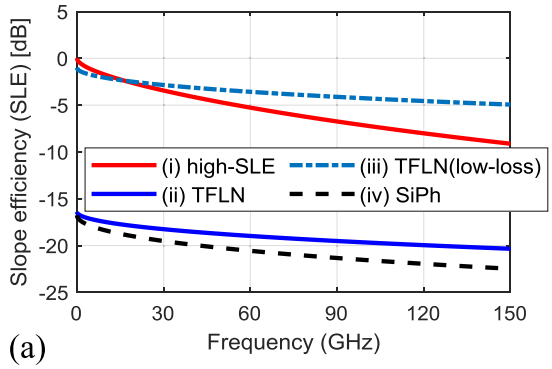

(a)

(b)	(i) High-SLE MZM	(ii) TFLN MZM [10, 29]	(iii) TFLN (low-loss) (hypothetical)	(iv) SiPh [16, 28, 32]
$V_{\pi 0}$ (V)	1.9	2.4	2.4	5.6
α_c ($cm^{-1}Hz^{-1/2}$)	6.8e-7	2.55e-6	2.55e-6	1.55e-5
α_d ($cm^{-1}Hz^{-1}$ or $cm^{-1}Hz^{-2}$)	1.8e-12	0	0	0
l_C (dB)	3.3	11	3.3	7.5
l_P (dB)	0.5	0	0	0
Length (cm)	5	1	1	0.25
Theoretical 3dB bandwidth (GHz) [30, 31, 39]	28	99	99	47

Fig. 2. (a) Theoretical SLE (in dB or 20·log10[$s_{MZM}(f)$], all normalized to case (i) at 1 kHz) of our high-SLE MZM, a TFLN MZM and a silicon photonic (SiPh) MZM. (b) Key parameters assumed. The 3 dB (EO) bandwidth calculation assumed a reference frequency of 5 GHz [30].

II. Theoretical Analysis of the Modulator's SLE and Device Design

A. Theoretical SLE of Modulators

In this sub-section, the modulator SLE as a FoM for low-RF-to-RF-loss, low-complexity IM-DD link design is discussed.

The frequency-dependent SLE of a traveling-wave MZM s_{MZM} (unit: W/A) is [21], [22], [23]:

$$s_{MZM}(f) = \frac{\pi}{2}\frac{P_{LD} R T_{ff}}{V_\pi(f)} \tag{1}$$

where P_{LD} (unit: W), R (unit: Ohm or Ω), T_{ff} (unit: 1) and $V_\pi(f)$ (unit: V) respectively represent the laser power, the source impedance, the fiber-to-fiber transmittance and the (frequency-dependent) half-wave voltage. SLE for optical modulators is derived assuming small-signal modulation and biasing at the quadrature point [22].

It can be seen that at the same P_{LD} the SLE is proportional to R and T_{ff}, while it is inverse proportional to $V_\pi(f)$. Here T_{ff} (<1) is in linear domain, while in the logarithm domain,

$$-T_{ff}\,(\mathrm{dB}) = l_C\,(\mathrm{dB}) + l_P\,(\mathrm{dB}) \tag{2}$$

Where l_C and l_P denote the coupling loss and the propagation loss of the modulator, respectively. The *RF-to-RF signal gain/loss G(f)* (unit: 1) of an IM-DD link, or the power ratio of an RF input and the corresponding output, is [23]

$$G(f) = s_{MZM}^2(f)\, r_{PD}^2(f) \tag{3}$$

Where r_{PD} (unit: A/W) is the responsivity of the photodetector (PD). In essence, higher G means a less-lossy electro-optical link, indicating less demand for OA and RFA and being helpful to operate with CMOS-class driving voltages. Here, we focus on the impact of modulator and assume the PD is ideal (e.g., r_{PD} is unity). In this case, SLE determines *G(f)*.

$V_\pi(f)$ is modelled as [26]

$$V_\pi(f) = V_{\pi 0}\cdot\frac{\alpha(f)\,L}{1-e^{-\alpha(f)L}} \tag{4}$$

Where $V_{\pi 0}$ (unit: V), α (unit: cm^{-1}), and L (unit: cm) denote direct-current (DC) V_π, microwave loss factor and MZM electrode length, respectively. The theoretical 3 dB bandwidth of the MZM can be calculated from $V_\pi(f)$ [31], [39]. $\alpha(f)$ mainly depends on the conductor loss α_c (unit: $cm^{-1}Hz^{-1/2}$) and the dielectric loss α_d; for example, in LN MZM case [27] (where α_d has a unit of $cm^{-1}Hz^{-1}$):

$$\alpha(f) = \alpha_c f^{1/2} + \alpha_d f \tag{5}$$

While in the case of SiPh MZMs [28] (where α_d has a unit of $cm^{-1}Hz^{-2}$):

$$\alpha(f) = \alpha_c f^{1/2} + \alpha_d f^2 \tag{6}$$

Here, we study theoretical SLE of different MZMs under the same P_{LD} and R. Fig. 2(a) shows the theoretical SLE in dB or 20·log10[$s_{MZM}(f)$] of 4 MZMs that achieved C-band >300 Gb/s bit-rate:

(i) our high-SLE MZM ($V_{\pi 0}$ = 1.9 V, l_C = 3.3 dB, lP = 0.5 dB);
(ii) a ∼100 GHz thin-film LN (TFLN) MZM [10], [29];
(iii) TFLN [10], [29] but with a hypothetical low l_C = 3.3 dB;
(iv) a 47 GHz SiPh MZM [16].

The key parameters assumed are summarized in Fig. 2(b). Please note that when a certain parameter is not available in the literature, we conservatively assume it toward the highest possible SLE. For example, α_d and l_P are assumed to be 0 in cases (ii)∼(iv). Besides, α_c value of the SiPh MZM is assumed so that its 3 dB bandwidth approximates the measured value of 47 GHz [16]. From Fig. 2(a) it can be observed that our MZM has a higher SLE at low frequencies, although its theoretical 3 dB bandwidth (shown in Fig. 2(b)) is not advantageous. As will be shown next, this yields competitive BER performance beneficial for an OA&RFA-free IM-DD link.

B. Theoretical Link Symbol/Bit Error Rate (SER/BER)

To derive the theoretical link SER/BER, we assume that fiber dispersion doesn't induce deep spectral notches and there's no OA or RFA. In such case, Gaussian approximation can be used for the theoretical derivation, i.e., assuming that the inter-symbol interference (ISI) caused by the channel can be approximated by equivalent non-fading additive Gaussian noise terms [33], [34]. It needs the calculation of discrete-time channel impulse response (CIR) $\{g_n\}$. If the signal baud-rate is B while Tx & Rx use ideal low-pass filters (LPF, cut-off at $B/2$), and Rx ideally samples at B, we have:

$$g_n = \mathcal{F}^{-1}\left\{\underbrace{H(f)}_{LPF}\ \underbrace{\sqrt{G(f)}}_{MZM\ \&\ PD}\ Re\left[\underbrace{e^{j2\pi^2 f^2 \beta_2 L_F}}_{fiber}\right]\right\} \quad (7)$$

where $\mathcal{F}^{-1}$ and "Re" denote inverse discrete-time Fourier transform and taking real-valued part, respectively [35]. For PAM-N format [36],

$$SER_{PAM-N} = (N-1)/N \cdot erfc\left(\sqrt{\frac{g_0^2/2}{(N^2-1)\sum_{i\neq 0} g_i^2/3 + N_0}}\right) \quad (8)$$

Where N_0 denotes the variance of the additive Gaussian noise component in the discrete-time channel model (see Appendix B for more details). If finite-length digital FFE is considered, we first derive the minimum mean-square-error (MMSE) FFE weight vector $\boldsymbol{c}$ using the orthogonality principle [37], [38], and the total impulse response vector $\boldsymbol{h}$ is obtained by discrete-time convolution:

$$\boldsymbol{h} = \boldsymbol{c} \otimes \boldsymbol{g} \quad (9)$$

And according to Refs. [36], [37],

$$SER_{PAM-N} = (N-1)/N \cdot erfc\left(\sqrt{\frac{h_0^2/2}{(N^2-1)\sum_{i\neq 0} h_i^2/3 + N_0 \sum c_i^2}}\right) \quad (10)$$

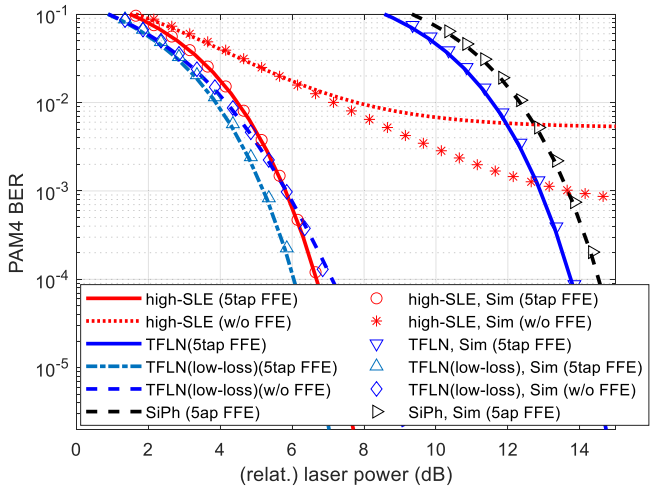

Fig. 3. Theoretical BERs and simulated BERs vs (relative) laser power of 150GBd PAM4 system with MZMs (i)∼(iv). The fiber dispersion was assumed to be 0 to emulate a short-reach transmission regime.

For more detailed derivations, readers may refer to Appendix B. Finally, assuming 1 bit error per symbol error (e.g., by Gray coding), BER of PAM-N can be derived from SER as $BER = SER/\log_2 N$.

Fig. 3 shows the theoretical and simulated BERs versus the (relative) laser power of an 150GBd PAM4 (300 Gb/s) IM-DD system with different MZMs (i)∼(iv). When digital FFE is used, the theory can predict the system BER performance with decent accuracy free from time-consuming Monte-Carlo simulations. Importantly, we can see that when digital FFE is used, our high-SLE MZM requires a relatively small laser power, or equivalently, less demand for optical/RF amplification at the same BER level.

C. MZM Device Design and Fabrication

To achieve a high slope efficiency (SLE) when designing the modulator, from (1), both a low V_π and a large T_{ff} (i.e., a small optical loss) are important. Our design considerations are from 3 aspects. (*i*) Choice of material and platform. We selected Ti-diffused LN platform featuring a large Pockels effect and low absorption in telecommunication wavelengths has an advantage in low V_π and optical loss. The MZM employed Ti diffusion on the x-cut LN layer bonded to the low dielectric constant handle wafer with a dielectric constant of less than 4 [39]. Fig. 4(a) shows the structure of the optical modulator. It consists of optical waveguides in Mach-Zehnder interferometric configuration, a traveling-wave RF electrode and a bias electrode. (*ii*) Choice of MZM electrode length. This depends on the relationship between optical propagation loss of the optical waveguide and electrode propagation loss at a given $V_{\pi 0}L$ product. Theoretically a length of around 5∼7 cm was found to be near-optimal for the SLE for a frequency of interest of 110 GHz. By also taking into account the limitation of our fabrication equipment, the length was designed to 5 cm. (*iii*) Consideration of device's cross-sectional structure. We applied a substrate consisting of a thinned LN layer and another low-dielectric-constant material layer, which mitigates frequency ripples due to mode coupling

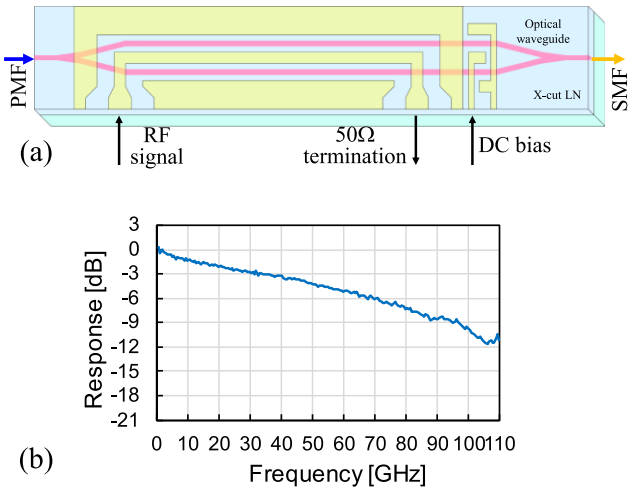

Fig. 4. (a) Structure of the designed optical modulator. PMF: polarization-maintaining fiber. SMF: single-mode fiber. (b) Measured EO response of the fabricated prototype.

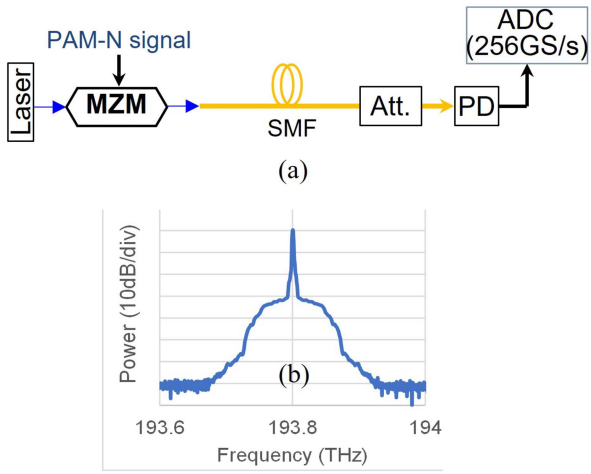

Fig. 5. (a) Experimental setup. Att.: optical attenuator. (b) An example of optical spectra of 128GBd PAM8 signal at the MZM output.

between coplanar-guided and substrate mode. Thereafter, we designed a coplanar waveguide with >10 μm-thick electrodes to increase the electrical signal propagation speed for velocity matching to optical signal, and in order to decrease the electrical propagation loss and thus reduce V_π at high frequencies. The coplanar waveguide structure was carefully designed to maintain both the velocity matching and the impedance matching conditions.

The measured frequency response of the fabricated MZM is shown in Fig. 4(b). The 3 dB and 10 dB bandwidth are about 30 GHz and 100 GHz respectively. The measured optical insertion loss at the maximum transmission point of the fabricated MZM at 1.55-μm (including fiber pigtails) is only about 3.8-dB. $V_{\pi 0}$ was about 1.9 V.

III. Experimental Setup, Results and Discussion

A. Experimental Setup

In this section, we present extensive experimental demosntrations of high-speed low-complexity IM-DD PAM transmission using the designed high-SLE MZM. The experimental setup is shown in Fig. 5(a). At the Tx side, electrical PAM-N signals with different symbol rates were generated from an arbitrary waveform generator (AWG, Keysight M8199A) using sampling rates up to 256 GS/s. The detailed Tx-side configuration, including possible DSP, are described in the following subsections. The V_{pp} of the signals up to 990-mV (i.e., "sub-1V" or "CMOS-compatible" driving voltage [8]) was adjusted by a Keysight M8158A remote head (RH). The signal was modulated onto a ~100 kHz-linewidth optical carrier (at 193.8-THz or 1546.92-nm, unless otherwise stated) via the fabricated single-drive high-SLE MZM biased at the quadrature point. Owing to the high SLE, an average >6-dBm Tx output (with modulation) was obtained with only 13-dBm laser power. In the current MZM prototype, the polarizer at the MZM waveguide input can tolerate up to 13-dBm power. Higher Tx output power is possible by using a high-power-tolerant polarizer and higher laser power. Fig. 5(b) shows an example of optical spectra of 128-GBd PAM8 signal measured at the MZM output.

The optical double-sideband (DSB) PAM signal was then transmitted over up-to-600 m G.652-compliant SMF. At the Rx side, the optical signal was power-attenuated, detected by a 50 GHz PD (in ≥408 Gb/s cases, a 70 GHz PD) and captured by a 256 GSa/s analog-to-digital converter (ADC, Keysight real-time oscilloscope). The reception was OA&RFA-less. The Rx-side offline processing includes resampling, digital LPF, down-sampling to 1 sample-per-symbol (SpS), symbol-spaced FFE or DFE, PAM-N demodulation and error counting. Throughout the section, "FFE{x}" denotes an FFE with x taps, while "DFE{x,y}" denotes an DFE with x feedforward (FF) filter taps and y feedback (FB) filter taps.

B. 224 Gb/s and 342 Gb/s Transmission Over C-Band 600 m

We first demonstrated a low-complexity net-200G/lane short-reach system, which is of potential interest for the scenarios of intra-DC 800GbE and 1.6TbE. In addition to the CMOS-driving operation and OA&RFA-less reception, the Rx-side DSP complexity can be very low. The baud-rate of the PAM4 signal was set to 112-GBd (AWG was sampled at 2-SpS or 224-GS/s) and the line rate was 224-Gb/s. There wasn't any Tx-side DSP such as RRC shaping or pre-equalization. At Rx side, the 9-tap digital LPF was operated at 3-SpS with a passband cutoff frequency of 70-GHz. We set the number of FFE taps to 5, 7 and 9, and measured the BER versus the V_{pp} of PAM4 signal in back-to-back transmission. As seen from Fig. 6(a), when 7-tap FFE was used, performance below the 5.8% KP4 FEC limit (BER = 2.3e-4 [40]) was achieved when V_{pp}≥400 mV, and the performance was improved with increased V_{pp} up to 800-mV. In the subsequent measurements, V_{pp} = 600-mV was applied which reserved certain performance margin for 600 m SMF transmission. The outer Optical Modulation Amplitude (OMAouter) is an important parameter for PAM4 signals in IEEE standards. Fig. 6(b) depicts the 112GBd PAM4 OMAouter versus V_{pp},

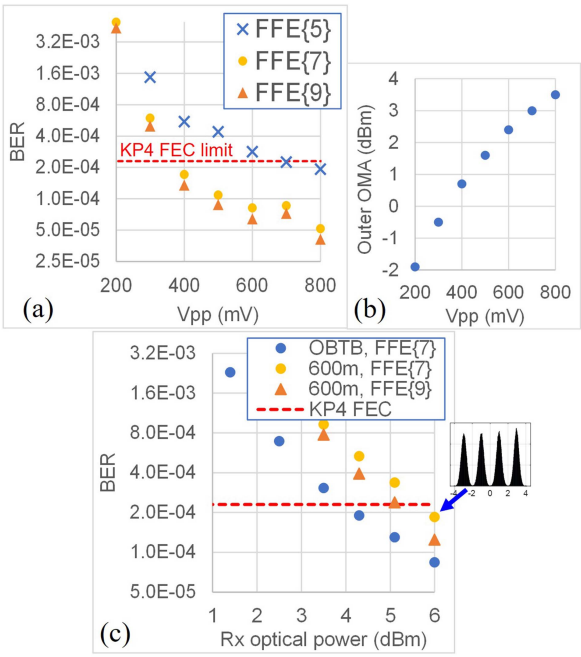

Fig. 6. Experimental results of 224 Gb/s PAM4 transmission. OBTB: optical back-to-back. (a) BER vs V_{pp} of RF signal in OBTB configuration; the received optical power was 6 dBm. (b) PAM4 outer OMA vs. V_{pp} of RF signal. (c) BER vs received optical power with V_{pp}=600-mV. The inset shows a sample PAM4 amplitude histogram.

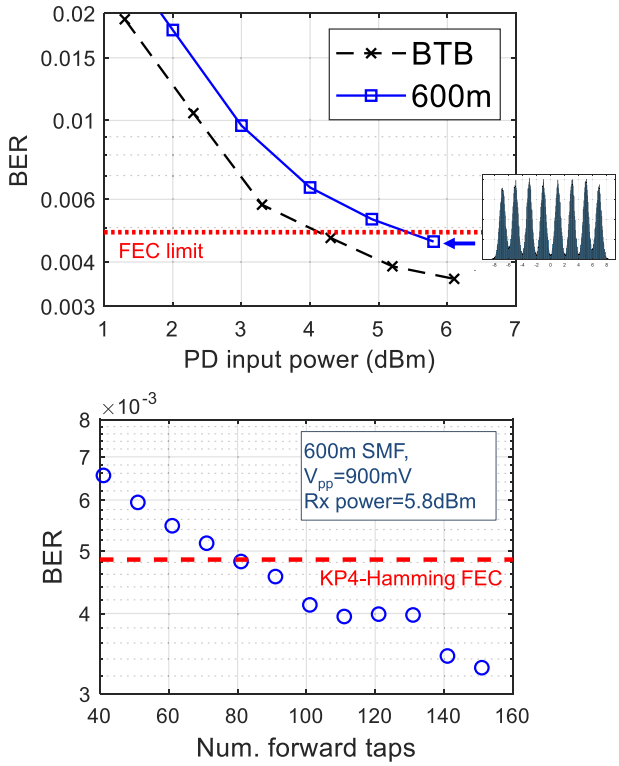

Fig. 7. 342-Gb/s PAM8 (net-302 Gb/s) experimental results. (a) BER vs. PD input power. The inset shows the amplitude histogram of the equalized PAM8 signal. (b) BER vs. number of FF filter taps in DFE.

measured at Tx output (attenuated to 3.5 dBm) by a Keysight N1000A sampling oscilloscope and a N1030A optical module. Besides, Transmitter and Dispersion Eye Closure Quaternary (TDECQ) at $V_{pp} = 600$ mV was 3.54 dB (measured with 60 GHz 4th-order Bessel filter, 9-tap reference FFE and target SER of 4.85e-3 [41], without any Tx-side digital/analog pre-equalizer or filters). Fig. 6(c) shows that the 224-Gb/s signal was successfully transmitted over 600 m in C-band with FFE{7}, while the power penalty compared with optical back-to-back (BTB) was around 1.6 dB, mainly due to the accumulated chromatic dispersion. A 9-tap FFE further improved the performance.

Next, we investigated the data rate of net-300G/lane with the same 600 m SMF distance. 114-GBd (342-Gb/s) PAM8 signal was applied without Tx DSP (AWG output at 2-SpS). The laser frequency in this experiment was 194.6-THz (∼1541 nm). The Rx-side digital LPF operated at 2-SpS with 10 taps and a passband cutoff frequency of 57-GHz. A higher-gain yet still practical KP4-Hamming concatenated FEC (12.9% overhead, with low latency & power [42]) was assumed, corresponding to a net data rate of 302 Gb/s after removing the FEC overhead. It was found that $V_{pp} = 900$ mV was sufficient to achieve a reasonable performance. Fig. 7(a) shows the BER versus the PD input power, when a DFE{91,1} was applied. After 600 m transmission, BER was below the FEC limit when the PD input power was 5.8-dBm. Fig. 7(b) shows the BER as a function of the number of FF filter taps in the DFE while the number of FB filter taps was limited to 1 for a sufficiently high circuit throughput [9]. Improved BER performance was observed with increased equalizer complexity. The relatively high number of FFE taps was related to both optoelectronic bandwidth limitations (considering the uncompensated AWG response, MZM's EO response and the PD bandwidth) and fiber dispersion.

C. Up-to-432 Gb/s Transmission

In this sub-section, we focused on higher data rates, namely up-to-432-Gb/s PAM8 transmission in C-band. Various symbol rates were investigated. When the symbol rate was 128-GBd or less, no Tx DSP was applied, and the AWG output the signal at 2-SpS using different DAC sampling rates; the signal V_{pp} (at RH output) was 900 mV; a 50 GHz *II-VI* PD was employed. The Rx-side digital LPF operated at 2-SpS, which had 10 taps and passband cutoff frequency fixed at half of the symbol rate.

On the other hand, for symbol rates higher than 128GBd, since we were operating at the bandwidth limit of the AWG M8199A, a digital RRC shaping filter (roll-off factor $\alpha = 0.02$) operating at 2-SpS was applied to the PAM signals before they were resampled to match the 256-GS/s AWG sampling rate. The signal V_{pp} was 990 mV. Besides, a 70 GHz PD was employed. In the Rx DSP, a matched RRC filter was used.

Fig. 8(a) shows the measured BER of systems with different gross bit rates, both in BTB and after 300 m. Different equalizers, namely DFE{81,1} and FFE{121}, were used as the signal bandwidth was different. Considering 16.7% HD-FEC limit [43], up to 384-Gb/s PAM8 was transmitted over 300 m successfully. Assuming 15.3% SD-FEC [44], 408-Gb/s (136-GBd) over 300 m and 420-Gb/s (140-GBd) in BTB transmission were

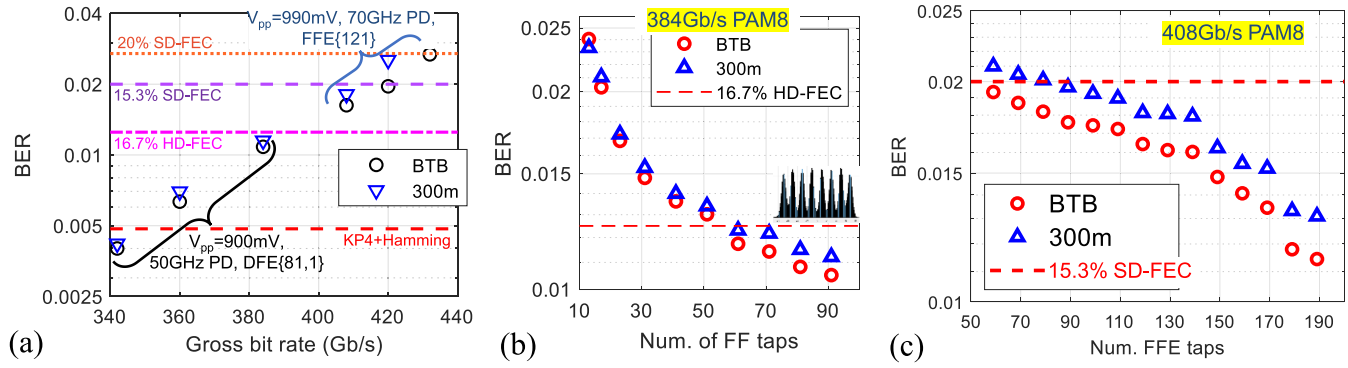

Fig. 8. Experimental results. (a) BER vs. gross bit rate of the IM-DD system. (b) BER vs. number of FF taps in DFE in 384-Gb/s PAM8 case. The inset shows PAM8 amplitude histogram with DFE{91,1}. (c) BER vs. number of FFE taps in 408-Gb/s PAM8 case.

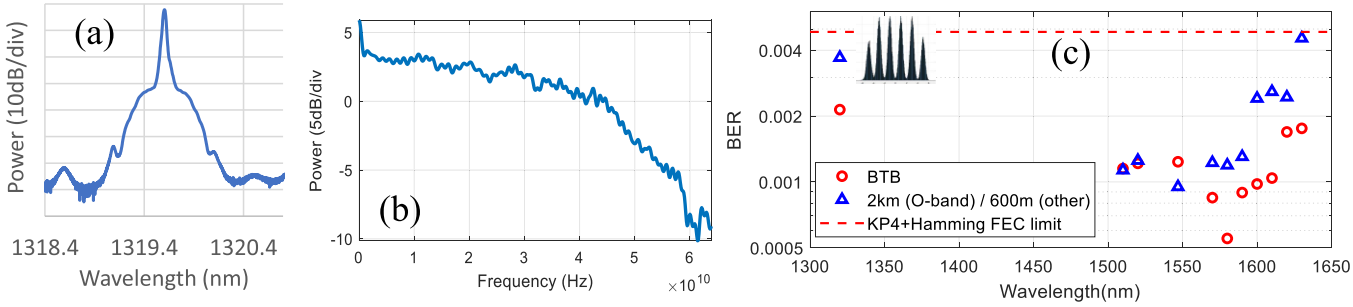

Fig. 9. Experimental results of O-band, S-band and L-band transmission. (a) Optical spectra of 128GBd (320 Gb/s) PAM6 signal at ∼1319.6 nm. (b) Corresponding channel frequency response. (c) BER measured over different wavelengths in O-, S-, C- and L-band. The inset shows an equalized amplitude histogram of 320 Gb/s PAM6 after 2 km transmission in O-band.

achieved. A 20% SD-FEC with BER threshold of 2.7e-2 [45] further enabled 420-Gb/s over 300 m, and 432-Gb/s (144-GBd) BTB transmission. It is worth noting that no complicated sequence detection such as MLSE was used; further symbol rate improvement was mainly limited by the analog bandwidth of the available AWG.

Next, we investigated the relationship between the equalizer complexity and the BER performance. Fig. 8(b) shows BER of Tx-DSP-free 384-Gb/s PAM8 signal as a function of the number of FF taps in the DFE. It is seen that DFE{61,1} enabled a BER lower than the 16.7% HD-FEC limit. Fig. 8(c) depicts BER of 408-Gb/s PAM8 signal as a function of the number of FFE taps. While 89 taps enabled a BER lower than the SD-FEC limit, more taps such as 179 taps further boosted the performance.

Soft-decision (SD)-FEC for long-haul coherent systems [44] can provide higher coding gain and tolerates higher BER. However, the decoding latency and power dissipation is the main concern. The SD-FEC thresholds assumed in this sub-section are just for performance benchmarking purposes. In practice, a distributed feedback (DFB) laser with a larger linewidth will likely be used yet with insignificant penalty considering the short reach [46].

D. Demonstration of High SLE Over O-, S-, and L-Band

One important merit of our modulator is that it does not rely on any resonant structure to enhance the efficiency [47], thereby it does not have the extra limitation on the operational optical wavelength. It has the potential of high-SLE operation over an ultra-wide optical bandwidth. In this subsection, we experimentally verified the OA&RFA-less reception of 850 mV-V_{pp} 128GBd (320 Gb/s) PAM6 signals over 2 km SMF in O-band and over 600 m SMF in S-, C- and L-band. The experimental setup was similar to Fig. 5(a). In O-band transmission case, we used a distributed feedback (DFB) laser with ∼1319.6 nm center wavelength, <10 MHz linewidth and ∼12.7 dBm output power. For S-band and L-band transmission, we used a Santec TSL-510 laser with a tunable range from 1510 nm to 1630 nm, linewidth of ∼500 kHz, and ∼12.8 dBm power. At the receiver, a 70 GHz PD was employed. In the Rx DSP, a 10-tap LPF (@ 2-SpS) with passband cutoff frequency of 64 GHz and a DFE{61,1} were employed. The optical loss of the high-SLE MZM in O-band, S-band and L-band was around 5∼6 dB depending on the wavelength.

Fig. 9(a) shows the optical spectra of the 320 Gb/s PAM6 signal at ∼1319.6 nm, while Fig. 9(b) shows the estimated channel frequency response with an end-to-end 3 dB bandwidth of about 40 GHz. The side-mode suppression of this DFB laser in this experiment was not as good as the C-band laser, which could cause certain capacity compromise. Nevertheless, as shown by Fig. 9(c), the signal was successfully transmitted over 2 km SMF in O-band assuming the KP4-Hamming FEC. The penalty was mainly due to the optical loss of the fiber and the connectors. We also tested S-band and L-band (from 1510 nm to 1630 nm)

transmissions over 600 m SMF, the results of which are shown in Fig. 9(c). Despite certain performance fluctuations which could be partially due to the different responsivity of the PD and possible imperfect manual tuning of bias voltages (optimal bias points were quite different for O-, S-, C- and L-band), the high-SLE MZM supported the transmissions at all wavelengths. The penalty at 1630 nm could be due to the characteristic of the available PD. (Note that, the nominal operational wavelength of this commercial PD from *II-VI Inc.* does not include either S-band or L-band.)

Nevertheless, we believe that our MZM can operate with high-SLE for an ultra-wide band, and the extension to other fiber bands (e.g., short-S-band or E-band) is only limited by the available laser and/or PD in this experiment.

IV. Conclusion

In this article, we have experimentally studied the feasibility of up-to-432 Gb/s PAM signal transmissions over 300 m/600 m SMF in C-band, 2 km in O-band, and 600 m in S- & L-band with sub-1V_{pp} driving voltages, OA&RFA-free reception, and low DSP complexity. A broadband MZM prototype, designed with high FoM of SLE, was the key to achieving these results. The experimental results are backed with a theoretical model of SLE and the IM-DD link; analytical results have been discussed. The presented high-SLE design path, analysis and experiments can potentially benefit the R&D of IM-DD links in future datacenter networks, business local area networks, mobile site cabling and so forth.

Appendix A
A Closed-Form Expression of the Discrete-Time CIR

Regarding the analysis in Section II-B, the closed-form expression of the discreate-time CIR $\{g_n\}$ could be of certain readers' interest. With Taylor expansion of (7)–(8) and approximations, one possible closed-form expression of $\{g_n\}$ is:

$$g_0 \approx \frac{\pi P_{LD}}{V_{\pi 0} I L_{ff}} \left\{ \frac{\left(L^2\alpha_c^2 - 3L\alpha_d\right) B}{8x} - \frac{L\alpha_c\sqrt{B}}{6\sqrt{2}} + \frac{1}{2} \right\} \tag{11}$$

$$g_{\pm n} \approx \frac{\pi P_{LD}}{B V_{\pi 0} I L_{ff}} \left\{ \begin{array}{l} \frac{A[cos(n\pi)-1]}{(2n\pi/B)^2} \\ + \frac{\sqrt{\pi} L\alpha_c \cdot S\left(\sqrt{2n}\right)}{2\sqrt{2}(2n\pi/B)^{\frac{3}{2}}} \end{array} \right\} \tag{12}$$

where $A = (L^2\alpha_c^2 - 3L\alpha_d)/x$ (e.g., $x = 40$) and $S(*)$ denotes the Fresnel Sine integral.

On the other hand, the derivation of the closed-form expression of $\{h_n\}$ which includes the impact of digital equalizers is also interesting, which may be a future work.

Appendix B
Derivation of (8) & (10)

We consider a discrete-time channel model with transmitted symbols $\{b_i\}$, received symbols $\{y_i\}$, channel impulse response $\{g_i\}$ and additive Gaussian noise component $\{n_i\}$.

$$y_i = \sum_{k=-\infty}^{\infty} b_k g_{i-k} + n_i = b_i g_0 + \sum_{k\neq i}^{\infty} b_k g_{i-k} + n_i \overset{\text{def}}{=} b_i g_0 + \upsilon_i \tag{13}$$

The SER of a PAM-N signal can be expressed as

$$SER_{PAM-N} = \begin{cases} \Pr\{\upsilon_i < -g_0\}, & b_i = N-1 \\ \Pr\{\upsilon_i > g_0\}, & b_i = -N+1 \\ \Pr\{\upsilon_i < -g_0\} + \Pr\{\upsilon_i > g_0\}, & otherwise \end{cases} \tag{14}$$

To derive SER, cumulative density function (CDF) of υ_i, i.e., $F_{\upsilon_i}(x) = \Pr\{\upsilon_i < x\}$, is needed. Under Gaussian approximation, the combined term υ_i is also zero-mean and Gaussian distributed with variance of σ_υ^2. Therefore,

$$\Pr\{\upsilon_i < -g_0\} = \Pr\{\upsilon_i > g_0\} = \frac{1}{2}\, erfc\left(\sqrt{\frac{g_0^2}{2\sigma_\upsilon^2}}\right)$$

$$= \frac{1}{2} erfc\left(\sqrt{\frac{g_0^2/2}{(N^2-1)\sum_{i\neq 0} g_i^2/3 + N_0}}\right) \tag{15}$$

Where N_0 represents the variance of $\{n_i\}$. Therefore,

$$SER_{PAM-N} = \frac{2N-2}{N}\ \Pr\{\upsilon_i < -g_0\}$$

$$= \frac{N-1}{N} \cdot erfc\left(\sqrt{\frac{g_0^2/2}{(N^2-1)\sum_{i\neq 0} g_i^2/3 + N_0}}\right) \tag{16}$$

If finite-length digital FFE $\{c_i\}$ is considered, assuming that the equalizer-output symbols are $\{z_i\}$ and total impulse response vector $\boldsymbol{h} = \boldsymbol{c} \otimes \boldsymbol{g}$ (i.e., discrete-time convolution), we have:

$$z_i = \sum_{k=-\infty}^{\infty} b_k h_{i-k} + \sum_{k\,=\,-\infty}^{\infty} n_k c_{i-k}$$

$$= b_i h_0 + \sum_{k\neq i}^{\infty} b_k h_{i-k} + \sum_{k=-\infty}^{\infty} n_k c_{i-k} \overset{\text{def}}{=} b_i h_0 + \xi_i \tag{17}$$

The variance of $\{\xi_i\}$ is $N_0 \sum c_i^2$ [37]. With Gaussian approximation, similarly, the SER is expressed as

$$SER_{PAM-N} = \frac{N-1}{N} \cdot erfc\left(\sqrt{\frac{h_0^2/2}{(N^2-1)\sum_{i\neq 0} h_i^2/3 + N_0 \sum c_i^2}}\right) \tag{18}$$

References

[1] K. Zhong, X. Zhou, J. Huo, C. Yu, C. Lu, and A. P. T. Lau, "Digital signal processing for short-reach optical communications: A review of current technologies and future trends," *J. Lightw. Technol.*, vol. 36, no. 2, pp. 377–400, Jan. 2018.

[2] H. Isono, "Latest standardization trend and future prospects for 800G/1.6T optical transceivers," *Proc. SPIE*, vol. 12429, pp. 45–51, 2023.

[3] D. Che and X. Chen, "Modulation format and digital signal processing for IM-DD optics at post-200G era," *J. Lightw. Technol.*, vol. 42, no. 2, pp. 588–605, Jan. 2024.

[4] D. Kong et al., "Intra-datacenter interconnects with a serialized silicon optical frequency comb modulator," *J. Lightw. Technol.*, vol. 38, no. 17, pp. 4677–4682, Sep. 2020.

[5] N.-P. Diamantopoulos et al., "60 GHz bandwidth directly modulated membrane III-V lasers on SiO2/Si," *J. Lightw. Technol.*, vol. 40, no. 10, pp. 3299–3306, May 2022.

[6] European Telecommunications Standards Institute (ETSI), "Fifth Generation Fixed Network (F5G); F5G Technology Landscape," ETSI GS F5G 003, V1.1.1, Sep. 2021.

[7] A. Tartaglia et al., "Perspectives for co-packaged optics in radio access networks," in *Proc. 23rd Int. Conf. Transparent Opt. Netw.*, 2023, pp. 1–7.

[8] C. Wang et al., "Integrated lithium niobate electro-optic modulators operating at CMOS-compatible voltages," *Nature*, vol. 562, pp. 101–112, 2018.

[9] Y. Lu and Y. Zhuang, "DSP and FEC considerations for 800GbE and 1.6TbE," 2022. [Online]. Available: www.ieee802.org/3/df/public/22_02/lu_3df_01b_220215.pdf

[10] X. Chen et al., "Single-wavelength and single-photodiode 700 gb/s entropy-loaded PS-256-QAM and 200-GBaud PS-PAM-16 transmission over 10-km SMF," in *Proc. Eur. Conf. Opt. Commun.*, 2020, pp. 1–4.

[11] D. Che and X. Chen, "Higher-order modulation vs faster-than-Nyquist PAM-4 for datacenter IM-DD optics: An AIR comparison under practical bandwidth limits," *J. Lightw. Technol.*, vol. 40, no. 10, pp. 3347–3357, May 2022.

[12] Q. Hu et al., "Ultrahigh-net-bitrate 363 gbit/s PAM-8 and 279 gbit/s polybinary optical transmission using plasmonic Mach-Zehnder modulator," *J. Lightw. Technol.*, vol. 40, no. 10, pp. 3338–3346, May 2022.

[13] J. Zhang et al., "Nonlinearity-aware PS-PAM-16 transmission for C-band net-300-gbit/s/λ short-reach optical interconnects with a single DAC," *Opt. Lett.*, vol. 47, no. 12, pp. 3035–3038, 2022.

[14] X. Fang, F. Yang, X. Chen, Y. Li, and F. Zhang, "Ultrahigh-speed optical interconnects with thin film lithium niobate modulator," *J. Lightw. Technol.*, vol. 41, no. 4, pp. 1207–1215, Feb. 2023.

[15] O. Ozolins et al., "Optical amplification-free 310/256 Gbaud OOK, 197/145 Gbaud PAM4, and 160/116 Gbaud PAM6 EML/DML-based data center links," in *Proc. Opt. Fiber Commun. Conf. Exhib.*, 2023, pp. 1–3.

[16] M. S. Alam, X. Li, M. Jacques, E. Berikaa, P.-C. Koh, and D. V. Plant, "Net 300 Gbps transmission over 2 km of SMF with a silicon photonic Mach-Zehnder modulator," *IEEE Photon. Technol. Lett.*, vol. 33, no. 24, pp. 1391–1394, Dec. 2021.

[17] E. Berikaa et al., "TFLN MZMs and next-gen DACs: Enabling beyond 400 Gbps IMDD O-band and C-band transmission," *IEEE Photon. Technol. Lett.*, vol. 35, no. 15, pp. 850–853, Aug. 2023.

[18] C. Eschenbaum et al., "Thermally stable Silicon-organic hybrid (SOH) Mach-Zehnder modulator for 140GBd PAM4 transmission with sub-1V drive signals," in *Proc. Eur. Conf. Opt. Commun.*, 2022, pp. 1–4.

[19] G. P. Agrawal and N. K. Dutta, *Semiconductor Lasers*, 2nd ed. New York, NY, USA: Van Nostrand Reinhold, 1993, pp. 55–70.

[20] C. H. Cox, G. E. Betts, and L. M. Johnson, "An analytic and experimental comparison of direct and external modulation in analog fiber-optic links," *IEEE Trans. Microw. Theory Techn.*, vol. 38, no. 5, pp. 501–509, May 1990.

[21] C. Cox, E. Ackerman, R. Helkey, and G. E. Betts, "Techniques and performance of intensity-modulation direct-detection analog optical links," *IEEE Trans. Microw. Theory Techn.*, vol. 45, no. 8, pp. 1375–1383, Aug. 1997.

[22] C. Cox, *Analog Optical Links Theory and Practice*. Cambridge, U.K.: Cambridge Univ. Press, 2004, pp. 20–49.

[23] C. H. Cox, E. I. Ackerman, G. E. Betts, and J. L. Prince, "Limits on the performance of RF-over-fiber links and their impact on device design," *IEEE Trans. Microw. Theory Techn.*, vol. 54, no. 2, pp. 906–920, Feb. 2006.

[24] H. Zeng, X. Liu, S. Megeed, N. Chand, and F. Effenberger, "Real-time demonstration of CPRI-compatible efficient mobile fronthaul using FPGA," *J. Lightw. Technol.*, vol. 35, no. 6, pp. 1241–1247, Mar. 2017.

[25] P. Zhu et al., "384 Gb/s PAM transmission with CMOS-class driving voltage, Optical & RF-amplifier-free reception and low-complexity DSP using a high-slope-efficiency modulator," in *Proc. Eur. Conf. Opt. Commun.*, 2023, Paper We.B.6.4.

[26] Z. Liu and D. Zhu, "The effect of conductor loss on half-wave voltage and modulation bandwidth of electro-optic modulators," *Chin. Opt. Lett.*, vol. 2, no. 10, pp. 586–589, 2004.

[27] Y. Yamaguchi et al., "Traveling-wave Mach-Zehnder modulator integrated with electro-optic frequency-domain equalizer for broadband modulation," *J. Lightw. Technol.*, vol. 41, no. 12, pp. 3883–3891, Jun. 2023.

[28] D. Patel et al., "Design, analysis, and transmission system performance of a 41 GHz silicon photonic modulator," *Opt. Exp.*, vol. 23, no. 11, pp. 14263–14287, 2015.

[29] D. Zhu et al., "Integrated photonics on thin-film lithium niobate," *Adv. Opt. Photon.*, vol. 13, no. 2, pp. 242–352, 2021.

[30] E. Berikaa, M. S. Alam, and D. Plant, "Net 400-gbps/λ IMDD transmission using a single-DAC DSP-free transmitter and a thin-film lithium niobate MZM," *Opt. Lett.*, vol. 47, no. 23, pp. 6273–6276, 2022.

[31] M. Zhang, C. Wang, P. Kharel, D. Zhu, and M. Loncar, "Integrated lithium niobate electro-optic modulators: When performance meets scalability," *Optica*, vol. 8, no. 5, pp. 652–667, 2021.

[32] M. S. Alam et al., "Net 220 Gbps IM-DD transmssion in O-band and C-band with silicon photonic traveling-wave MZM," *J. Lightw. Technol.*, vol. 39, no. 13, pp. 4270–4278, Jul. 2021.

[33] P. Monsen, "Theoretical and measured performance of a DFE modem on a fading multipath channel," *IEEE Trans. Commun.*, vol. 25, no. 10, pp. 1144–1153, Oct. 1977.

[34] J. E. Smee and N. C. Beaulieu, "Error-rate evaluation of linear equalization and decision feedback equalization with error propagation," *IEEE Trans. Commun.*, vol. 46, no. 5, pp. 656–665, May 1998.

[35] A. Oppenheim and R. Schafer, *Discrete-Time Signal Processing*, 3rd ed. London, U.K.: Pearson, 2014.

[36] J. Weng and T. Le-Ngoc, "Performance analysis of M-PAM signalling with Tomlinson Harashima precoding over ISI channels," in *Proc. GlobeCom*, 2002, pp. 1–3.

[37] J. Proakis et al., *Digital Communications*, 5th ed. New York, NY, USA: McGraw-Hill, 2008.

[38] P. Zhu, Y. Yoshida, A. Kanno, and K. Kitayama, "Analysis and demonstration of low-complexity joint optical-electrical feedforward equalization (OE-FFE) for dispersion-limited high-speed IM/DD transmission," *J. Lightw. Technol.*, vol. 41, no. 2, pp. 477–488, Jan. 2023.

[39] P. T. Dat et al., "Transparent fiber-millimeter-wave-fiber system in 100-GHz band using optical modulator and photonic down-conversion," *J. Lightw. Technol.*, vol. 40, no. 5, pp. 1483–1493, Mar. 2022.

[40] R. Nagarajan, I. Lyubomirsky, and O. Agazzi, "Low power DSP-based transceivers for data center optical fiber communications," *J. Lightw. Technol.*, vol. 39, no. 16, pp. 5221–5231, Aug. 2021.

[41] A. Uchiyama et al., "225Gb/s PAM4 2 km and 10 km transmission of electro-absorption modulator integrated laser with hybrid waveguide structure for 800 Gb/s and 1.6 Tb/s transceivers," *J. Lightw. Technol.*, vol. 42, no. 4, pp. 1225–1230, Feb. 2024.

[42] X. Zhou, C. F. Lam, R. Urata, and H. Liu, "State-of-the-art 800G/1.6T datacom interconnects and outlook for 3.2T," in *Proc. Opt. Fiber Commun. Conf. Exhib.*, 2023, pp. 1–3.

[43] L. M. Zhang and F. Kschischang, "Staircase codes with 6% to 33% overhead," *J. Lightw. Technol.*, vol. 32, no. 10, pp. 1999–2002, May 2014.

[44] Open ZR+ MSA technical specification. OpenZR+ specifications, version 1.0. 2020. [Online]. Available: http://openzrplus.org/

[45] D. Chang et al., "LDPC convolutional codes using layered decoding algorithm for high speed coherent optical transmission," in *Proc. OFC/NFOEC*, 2012, pp. 1–3.

[46] A. Yekani and L. Rusch, "Interplay of bit rate, linewidth, bandwidth, and reach on optical DMT and PAM with IMDD," *IEEE Trans. Commun.*, vol. 67, no. 4, pp. 2908–2913, Apr. 2019.

[47] C. Han et al., "Slow-light silicon modulator with 110-GHz bandwidth," *Sci. Adv.*, vol. 9, 2023, Art. no. eadi5339.